

Green Chemistry

Accepted Manuscript



This is an *Accepted Manuscript*, which has been through the Royal Society of Chemistry peer review process and has been accepted for publication.

Accepted Manuscripts are published online shortly after acceptance, before technical editing, formatting and proof reading. Using this free service, authors can make their results available to the community, in citable form, before we publish the edited article. We will replace this *Accepted Manuscript* with the edited and formatted *Advance Article* as soon as it is available.

You can find more information about *Accepted Manuscripts* in the [Information for Authors](#).

Please note that technical editing may introduce minor changes to the text and/or graphics, which may alter content. The journal's standard [Terms & Conditions](#) and the [Ethical guidelines](#) still apply. In no event shall the Royal Society of Chemistry be held responsible for any errors or omissions in this *Accepted Manuscript* or any consequences arising from the use of any information it contains.

1 An Integrated Biorefinery Concept for Olive Mill Waste Management: Supercritical 2 CO₂ Extraction and Energy Recovery

3
4 Andrea Schievano^{1*}, Fabrizio Adani^{1*}, Li Buessing², Alfonso Botto³, Esteve N.
5 Casoliba⁴, Mara Rossoni¹, Jillian L. Goldfarb⁵

- 6
7 1. Dipartimento di Scienze Agrarie ed Ambientali (DISAA), Università degli Studi di
8 Milano, via Celoria 2, 20133 Milano, Italia
9 2. Department of Chemical Engineering, University of New Hampshire, 33 Academic Way,
10 Durham, NH 03824, USA
11 3. Separeco S.r.l., via Rivarossa 15, 10060 Piscina (TO), Italy
12 4. Veolia Water Solutions & Technologies, 4760 World Houston Parkway, Ste. 140,
13 Houston, TX 77032, USA
14 5. Department of Mechanical Engineering and Division of Materials Science &
15 Engineering, Boston University, 110 Cummington Mall, Boston, MA 02215, USA
16

17 Abstract

18 Commercial production of olive oil generates four times the amount of waste as it does
19 oil, along with a number of environmental issues. We propose an integrated biorefinery
20 concept for the management of pomace, i.e. solid Olive Mill Waste (OMW), that utilizes
21 supercritical carbon dioxide (SCO₂), coupled with a polar co-solvent (Ethanol), for
22 extracting value-added polyphenols and mono/poly-unsaturated fatty acids
23 (MUFA/PUFA), followed by thermochemical (oxidation or pyrolysis) recovery of
24 energy, biofuels and materials.

25 The SCO₂+EtOH extraction recovered 77.6 g of freeze-dried extract per kg of raw OMW,
26 with relatively high concentrations in polyphenols (10.9 g kg⁻¹ of which 60.1% of di-
27 hydroxytyrosol), PUFA (20 g kg⁻¹), MUFA (601 g kg⁻¹) and other valuable compounds,
28 such as squalene (10 g kg⁻¹). All these substances are of extreme interest in
29 pharmaceutical and nutraceutical market, for their antioxidant, anti-cancer, functional,
30 anti-bacterial and nutritional properties.

31 The SCO₂+EtOH flux acted as physical/chemical carrier for over 85% of humidity,
32 leaving the exhaust OMW almost dry, with evident advantages for downstream. Using
33 nonisothermal thermogravimetric analysis, the apparent activation energies required to
34 pyrolyze OMW to produce fuel and biochar ranged from 20 to 140 kJ/mol depending on
35 heating ramp rate and temperature regime. BET analysis of unactivated biochars show
36 increased (+25%) mesopore surface areas after SCO₂ extractions (up to 500 m²/g).
37 A more in-depth view on the proposed biorefinery is needed, to consider the overall
38 energy balance, as well as possible market values of the obtained extract, and evaluate the
39 real feasibility of the proposed concept.
40

41 Keywords

42 Biorefinery; Olive Mill Waste; Supercritical Fluid Extraction; Polyphenols; Squalene;
43 Pyrolysis; Oxidation; Biochar
44

45 *Corresponding authors: Andrea Schievano, andrea.schievano@unimi.it; Fabrizio Adani,
46 fabrizio.adani@unimi.it

47 Introduction

48 According to the International Olive Council (IOC), the global production of olive oil
49 reached 2.9 million metric tons in the 2012-2013 harvest ¹. The Mediterranean Basin and
50 the Middle East accounted for 95.9% of the total world olive oil production in this
51 harvest (latest available data), with Spain alone accounting for nearly 34% of the total
52 global production ¹. The commercial production of olive oil generates upwards of four
53 times the amount of waste as it does oil, representing a heavy burden on the olive oil
54 industry, a threat to the environment, and the potential waste of a useable series of
55 byproducts. The majority of olive mills utilize a three-phase centrifugation system,
56 introduced in the 1970s, that requires large amounts of water and produces two types of
57 waste: one in the form of a wastewater, known as olive mill wastewater, black water, or
58 alpechin, and the other in the form of a solid waste, known as pomace, or sansa ²,
59 hereafter called olive mill waste (OMW). These systems and types of waste are one of the
60 most diffuse in the Mediterranean area ³.

61 A variety of sources demonstrate the high and variable – from 0.02 g/kg up to 10 g/kg –
62 amounts of biophenols (*e.g.* hydroxytyrosol, tyrosol, caffeic acid, rutin, luteolin,
63 flavonoids) present in OMW that vary seasonally and geographically, and depend on the
64 type of milling ^{4,5}. The polyphenols present in olives and in olive oil are known to have
65 anti-oxidant, anti-inflammatory and anti-microbial properties ⁶. Most of them are
66 insoluble in oil and thereby remain in OMW and in wastewaters ⁶. It is these biophenols
67 that may hamper efforts to dispose of OMW and treat wastewater; high concentrations of
68 phenolic compounds can be phytotoxic and bacteriostatic ⁷. In many regions of Europe,
69 both OMW and wastewaters are often spread directly on land as fertilizers. Low
70 concentrations of OMW in soils have been observed in some cases to increase the organic
71 carbon, aggregate stability, available potassium, and cation-exchange capacity of soil, all
72 of which aid crop production ⁸. On the other hand, especially when large amounts of such
73 material are used in soil, the net effect on crops and on soil micro flora is questionable,
74 given the toxicity at high doses ⁹.

75 At the same time, one of the primary biophenols present, hydroxytyrosol, retails for
76 upwards of \$500 (U.S.) for 100 mg at 98% purity ¹⁰. Nutraceutical products like capsules
77 with extracted concentrates from olives and/or olive-tree fractions may reach market

78 prices of around 100-200 € for 100 mg of hydroxytyrosol ¹¹. Removing these biophenols
79 from OMW solves the phytotoxic disposal issue as well as provides a revenue stream for
80 the use of polyphenols in the health food, cosmetic, and pharmaceutical industries ¹².
81 Moreover, other interesting and valuable compounds can be extracted from OMW,
82 especially regarding the fat fractions, rich unsaturated fatty acids (UFA) and squalene ¹².
83 Squalene, in particular, is an intermediate metabolite in the synthesis of cholesterol and
84 phytosterols. In humans, about 60% of dietary squalene is absorbed and is distributed
85 ubiquitously in tissues, being one of the major components of the epidermal lipids.
86 Supplementation of the diet with squalene can reduce cholesterol and triglyceride levels.
87 Acting as a quencher of singlet oxygen, squalene functions in protecting skin surface
88 from lipid peroxidation ¹³.
89 There are several methods under consideration for the extraction of biophenols, UFA and
90 squalene from olive byproducts. From olive mill wastewaters, the main separation
91 strategy involves the use of successive micro- and nano-membrane filtrations ¹⁴. The
92 concentrated sludge must undergo further extraction and refinement processes, similarly
93 to those used for OMW. These methods include ultrasound-assisted extraction ¹⁵; solvent
94 extraction ¹⁶; superheated liquid extraction ¹⁷ and supercritical fluid extraction ¹⁸.
95 The difficulty in separating phenolic compounds from the waste comes from the
96 hydrophilic and amphiphilic natures of the phenolic compounds. Supercritical fluid
97 extraction is suitable for extracting molecules for human consumption because it
98 eliminates the harsh solvents used in conventional extractions. CO₂ is the most common
99 supercritical fluid used because it is a nontoxic, nonflammable, widely available and
100 inexpensive at high purity solvent, exhibiting moderate critical conditions (31.1°C and
101 73.8 MPa) and can be easily separated because of its high volatility at normal conditions
102 ¹⁹. There are several advantages to Supercritical Carbon Dioxide (hereafter SCO₂) over
103 organic solvent extraction. The first is solvency power, which can be changed easily by
104 adjusting operating conditions (temperature and pressure), which in turn change the
105 extraction capacity and selectivity to extract the desired compounds. The near ambient
106 temperatures at which SCO₂ proceeds gives it the advantage over conventional solvent
107 methods run at higher temperatures, as there is less thermal stress on the desired extract
108 ²⁰. The main issue with SCO₂ is that it is usually limited to low or medium polarity

109 compounds due to the low polarity of CO₂. A co-solvent (modifier) can increase
110 extraction efficiency immensely and can be used to reduce operating pressure, extraction
111 time, and also for extraction of polar compounds²¹. The most common co-solvents are
112 ethanol and methanol. Le Floch¹⁸ found methanol to be a better co-solvent than ethanol
113 for extracting polyphenols from olive leaves, but due to the toxicity of methanol, ethanol
114 is preferred for downstream human consumption. The extracted compound yield
115 increases with constant temperature and increasing pressure, but decreases with
116 increasing temperature at constant pressure due to the solvent density reduction²².
117 While mitigating the phytotoxicity of OMW by polyphenols extraction would enable
118 more widespread use as a soil amendment, the vast quantities of OMW produced over a
119 short time (3-4 month harvest) suggest that using extracted OMW as a fertilizer cannot be
120 the sole method of disposal unless the waste is transported long distances to agricultural
121 sites, thus increasing both costs and the carbon footprint of the waste^{23,24}. There are
122 several viable bioenergy conversion pathways to consider with the OMW following
123 SCO₂, as seen in Figure 1.

124 One disposal method that is of interest in some locations is combustion of OMW. For
125 centralized olive oil production facilities, where vast quantities of OMW are produced
126 and land application is not an option, this process reduces the amount of waste disposed
127 via oxidation, using the heat from combustion for evaporation of the humidity of the
128 incoming waste streams and for other purposes²⁵. Combustion reduces the quantity of
129 waste, but the extent of combustion, the profile of volatilized compounds, and the
130 disposal of ash must all be addressed to insure that this process is industrially and
131 environmentally feasible.

132 Another pathway that we consider here is the pyrolysis of OMW. Pyrolysis (heating in
133 the absence of oxygen) can be used to produce a bio-oil or syngas that mimics petroleum-
134 derived fuels, and a carbonaceous char with high specific surface areas²⁶. The
135 temperature and heating rate of pyrolysis strongly affects the quantities of each product
136 (bio-oil, syngas, char) recovered²⁷, and the development of industrial devolatilization
137 units requires a complete understanding of pollutant evolution and kinetics modeling²⁸.
138 There has been a significant amount of work done on the pyrolysis of raw OMW and
139 OMW mixed with various other waste products^{27, 29, 30, 31, 32, 33, 34}. The calorific value of

140 bio-oil extracted from raw OMW was found to be as high as 29MJ/kg with a molecular
141 formula of $\text{CH}_{1.54}\text{N}_{0.02}\text{O}_{0.29}$, with maximum oil yield from fast pyrolysis at approximately
142 550°C (E.U. 2011). Syngas produced from OMW pyrolyzed at 550°C by Uzun³⁵ was
143 shown to contain approximately 50% CO_2 , 14% CO , 21% H_2 , balance roughly split
144 between CH_4 , C_2H_4 and C_2H_6 . However, overall little research has been done on such an
145 integrated pathway, considering the changes in thermal decomposition of OMW
146 following SCO_2 .

147 In this work, we explore an integrated biorefinery concept (Figure 1) that aims to produce
148 value-added products (high value antioxidants, biofuels, energy, sustainable source of
149 carbon for soil) and at the same time solve concerns over the proper disposal of OMW.
150 This new approach would further “green” the ancient practice of olive oil extraction.

151

152 **Results and discussion**

153 The total content of dry matter (DM) in fresh matter (FM), organic matter and ash in the
154 raw OMW were 660, 587 and 63 $\text{g kg}^{-1}\text{FM}$; total polyphenols (TP) content was 1.809 g
155 kg^{-1}FM (Table 1).

156 *SCO₂ extractions from OMW*

157 The mass balance of FM, DM and TP of the two extractions performed are reported in
158 Table 1. SCO_2 resulted in two separate phases: one aqueous and the second fat-like. The
159 transport of water by the CO_2 stream is related to a physical phenomenon (induced by
160 pressure, heat and flux), while the fat fraction transport is both physical and chemical in
161 nature (SCO_2 behaves like a non-polar solvent), as indicated by Adani³⁶. Together, these
162 two fractions accounted for 16.3% of initial FM and for 8.4% of initial DM (Table 1).

163 Over 83% and 91% of initial FM and DM, respectively, were left in the exhaust OMW,
164 while a negligible fraction was lost within the circuit (Table 1). The OMW was left
165 relatively humid after extraction (Table 1).

166 In SCO_2+EtOH , the aqueous and fat fractions were extracted as a homogeneous
167 emulsion, probably attributed to the polar action of ethanol. For the same reason, the
168 extraction and transport of the aqueous phase was more efficient (over 85% removal of
169 initial moisture content) and the exhaust OMW remained almost dry at the end of the
170 SCO_2+EtOH ($947 \text{ gDM kg}^{-1}\text{FM}$, Table 1); the emulsion weighted almost 50% of the

171 initial mass (including ethanol), with negligible losses (Table 1). At the same time,
172 similarly to SCO_2 , the extracted DM represented 11.7% of the initial DM, while 86.8% of
173 it remained in the exhaust.

174 Notable differences between SCO_2 and SCO_2+EtOH were observed for TP extraction; it
175 exceeded 45% yield in the extract of SCO_2+EtOH , while very weak extraction yields
176 were achieved by SCO_2 , with 97% of the TP left in the exhaust OMW (Table 1). Both
177 extracts, when freeze-dried, accounted for 5-6% by mass of the initial OMW and, while
178 the SCO_2 extract showed a TP concentration of $0.967 \text{ gGAE kg}^{-1}$, the SCO_2+EtOH
179 reached $10.86 \text{ gGAE kg}^{-1}$.

180 Phenolic compound speciation indicated that di-hydroxytyrosol accounted for over 50%
181 of TP in both extracts (Table 2). At the same time, the relative percentages of single
182 phenolic compounds were similar in both extractions, though in SCO_2+EtOH all of them
183 were nearly 10 times more concentrated than SCO_2 alone (Table 2).

184 Both extracts were substantially composed of fats (as all fatty acids and esters were
185 converted into FAMEs before analysis, total FAME represented over 90% of DM, Table
186 2) and both of them composed of over 60% elaidate (i.e. a trans-isomer of oleate) and
187 palmitate, while the rest was composed of 10 main compounds, as shown by the FAME
188 speciation (Table 2). Mono-unsaturated (MU) and poly-unsaturated (PU) fatty acids (FA)
189 were a considerable fraction of the fats, i.e. nearly $600 \text{ g kg}^{-1}\text{DM}$ in both extracts (Table
190 2).

191 Among them, some compounds of particular interest were found in relevant
192 concentrations: linoleate and cis-vaccenic acid were found in similar concentrations in
193 both extracts (around 20 and $70 \text{ g kg}^{-1}\text{DM}$, respectively, Table 2). Squalene
194 (2,6,10,15,19,23-hexamethyl tetracosaeheptaene) was also detected at concentrations of
195 21 and $10 \text{ g kg}^{-1}\text{DM}$ in SCO_2 and SCO_2+EtOH , respectively.

196 Of the two options of SCO_2 investigated, coupling EtOH to CO_2 resulted in enhancing,
197 by a factor of 10, the extraction of phenolic compounds (Table 1 and 2), while no
198 significant differences were observed in extracting the fat fractions (Table 2). This was
199 expected; a supercritical CO_2 stream alone is known to possess the capability of
200 extracting and transporting non-polar compounds, such as fats, and to have less of an
201 effect on polar molecules, such as phenols²¹. The addition of EtOH as a co-solvent

202 optimized phenolic transport to the supercritical fluid phase. On the other hand, EtOH
203 addition simultaneously resulted in a massive transport of the initial moisture of OMW,
204 with the exhaust OMW left nearly dried and the extract with over 50% water content
205 (Table 1). This, in a scaled-up process, would impose higher energy requirement to dry or
206 freeze-dry the extract, as compared to SCO₂, where the moisture content of the extract
207 was around 20% (Table 1). However, SCO₂ alone was not sufficient to achieve
208 satisfactory extraction of the polyphenols (Table 1).

209 The compositions of both extracts in terms of FAME were found similar to typical olive
210 oil³⁷. Elaidate is the trans-isomer of oleate and, together with palmitate, represented the
211 large majority of both extracts. Squalene, well known for showing important anti-tumor,
212 anti-oxidant and functional activity in the human body¹², was also found in relatively
213 high concentrations (10-20 g kg⁻¹DM, Table 2), when compared with typical
214 concentrations found in literature for olive oils (4-10 g kg⁻¹ of olive oil)³⁸. This is
215 regardless of the use of EtOH in the extraction, Squalene being soluble in solvents like
216 hexane or SCO₂ (Table 2).

217

218 *Kinetics of Oxidation and Pyrolysis of Raw and Treated OMW*

219 As seen in Table 3, the impact of extraction on total elemental composition of carbon,
220 hydrogen and nitrogen, by mass, was minimal and close to standard experimental errors
221 of ±0.4%. This suggests that the thermal reactivities of the materials should be similar.
222 Experiments were conducted to determine the impact of extraction treatment on the
223 pyrolysis and oxidation kinetics; two particle sizes (125-300 μm and 300-500 μm) were
224 analyzed to further probe the effect of particle size on the apparent activation energy. It
225 was observed by Van de Velden³⁹ that there are mass transfer limitations in the pyrolysis
226 of larger particles as larger particles and higher heating rates cause a temperature gradient
227 from the outside to the center of the particle. Figure 2 is a representative
228 thermogravimetric (TG) curve with an inset derivative thermogravimetric (DTG) curve
229 for the pyrolysis of raw OMW at each particle size and heating ramp rate used. We
230 clearly see from these results that the kinetics of thermal decomposition is significantly
231 influenced by the heating rate and to a lesser extent by the particle size (Figure 2). Table
232 4 presents the peak mass loss temperature and rate (determined through DTG curves of

233 each sample, as shown the Supplemental Materials in Tables S1-S4 and Figures S2 and
234 S3) for each sample. We see that the peak DTG points occur within approximately 600-
235 630K for pyrolysis, and 550-580K for oxidation. For both pyrolysis and oxidation, the
236 higher heating rates display higher peak temperatures (on the order of ~20K higher for
237 each sample), no matter the particle size. Figure 3 illustrates the DTG curves of oxidation
238 for the raw and extracted OMW samples at 100K/min for small and larger particles; we
239 note the shapes of the DTG curves are similar for each sample, but that the maximum rate
240 of mass loss is higher for the smaller particle sizes. Both of these observations point to
241 clear heat and mass transport limitations: higher heating rates result in higher peak mass
242 loss temperatures and bigger particles lead to lower peak mass loss rates. Therefore, we
243 note that the activation energies presented herein are “global” or “apparent” activation
244 energies, encompassing these transport limitations within the reaction chemistry to
245 provide “lumped” activation energy of the particles in question and the applied heating
246 rate. Jauhiainen⁴⁰ presented a thorough discussion on the simultaneous decomposition of
247 biomass in the context of OMW pyrolysis and oxidation in an attempt to explain some of
248 the TG and DTG behavior of OMW conversion. Ounas⁴¹ found similar TG behavior for
249 the pyrolysis of olive residue at heating rates ranging from 2 to 50 K/min as we observe
250 here. The extraction treatment does not appear to largely impact the DTG results, though
251 we do observe a significant impact of extraction treatment on the global activation
252 energies of pyrolysis and oxidation for the OMW, despite these potential heat and mass
253 transfer limitations.

254 For both pyrolysis and oxidation, we see three mass loss regimes (Table 4), or distinct
255 regions on the Arrhenius plots, characterized by linear $\ln k$ vs. $1/T$ portions with abrupt
256 discontinuities. This behavior was observed by many across the biomass literature for
257 both pyrolysis and combustion processes^{32,39,42, 43}. The temperatures at which these
258 discontinuities occur are relatively independent of particle size and heating rate for
259 pyrolysis, and are strongly influenced by heating rate during oxidation, as seen in Table 4
260 and Figures 4 and 5. We have labeled each of these discrete sections “Mass Loss
261 Regimes.” For pyrolysis of lignocellulosic materials, these three regimes are often
262 roughly attributed to the decomposition of hemicellulose, cellulose and lignin, and for the
263 oxidation process to the pyrolysis of volatiles, followed by the oxidation of these volatiles

264 and finally resulting char oxidation. The activation energies of pyrolysis ranged from
265 57.7-74.5 kJ/mole in regime 1, from 56.9-87.6 kJ/mole in regime 2, and 3.4-30.4 in
266 regime 3. In their pyrolysis of solid OMW, Taralas⁴⁴ reported an overall activation
267 energy of approximately 90 kJ/mol for particles between 0.5 and 1mm up to 975K. Ounas
268⁴¹ reported activation energies obtained from the Ozawa-Flynn-Wall and Vyazovkin
269 methods for fractional conversions of OMW ranging from 148-219 kJ/mol pyrolyzed at
270 2, 10, 20 and 50 K/min with an average particle size of 0.2mm. Jauhiainen⁴⁰ find two
271 different mass loss regimes for the pyrolysis under helium at 5, 10 and 20 K/min of olive
272 mill stones, ranging from 69.4-181.8 kJ/mol using a modified Arrhenius equation that
273 optimizes the pre-exponential factor and kinetic constant at a given temperature using a
274 fourth-order Runge-Kutta method. They do not report a particle size.

275 In the low temperature mass loss regime, the raw untreated OMW showed approximately
276 10% higher apparent activation energy for pyrolysis than SCO_2 or SCO_2+EtOH in the
277 first and second mass loss regimes (Table 4). It is plausible that the hemicellulosic
278 materials were physically and chemically disrupted, and/or the removal of the fat
279 fractions (see DM balance in Table 1) decreased the apparent activation energies of the
280 treated materials; given scant qualitative evidence on SEM imaging (Figure 6) this is
281 likely a chemically induced transformation, though as the elemental distribution of C,H,N
282 across samples is similar (Table 3) it seems possible that polymeric cellulose chains were
283 disrupted. In fact, an emerging topic in the biomass to bioenergy conversion literature is
284 the variety of potential pretreatment options to enhance digestibility of lignocellulosic
285 materials⁴⁵ and CO_2 “explosion pretreatment” (SCO_2 at approximately 200°C, 1000-
286 4000 psi, i.e. at higher temperature than here) has been shown to form carbonic acid,
287 which hydrolyzes hemicellulose, and also increases the accessible surface area of the
288 biomass⁴⁶, lending credence to the more chemically induced nature of this treatment.

289 In the third (high temperature) pyrolysis mass loss regime we see a distinct effect of
290 particle size and heating rate on the predominantly lignin decomposition. The apparent
291 activation energies of the larger particles are up to twice as big as the smaller particles,
292 likewise the slower heating rate has substantially lower activation energy for each particle
293 size. In this case, the activation energy (for the same particle size/heating rate) is higher
294 for the SCO_2+EtOH than for the SCO_2 , which is higher than the raw OMW. This

295 indicates a high likelihood that the SCO_2 and SCO_2+EtOH pre-treatment effect only the
296 cellulose and hemicellulose portions of the OMW. Lignin is known to decompose from
297 ~ 190 to 600°C ; at lower temperature regimes the raw OMW is likely decomposing more
298 lignin, as it is the “glue” that holds together the cellulose and hemicellulose. This “glue”
299 was likely disrupted by hemicellulose hydrolysis during SCO_2 treatment, thereby
300 condensing the lignin together and causing a more energy-intensive, delayed
301 decomposition at higher temperature.

302 The effect of extraction treatment is somewhat more limited on the oxidation kinetics of
303 the OMW. The activation energies, with the exception of the raw OMW 125-300 μm ,
304 $100^\circ\text{C}/\text{min}$ sample, were all within ~ 25 kJ/mol of each other as seen in Table 4. The first
305 and third mass loss regimes – representing devolatilization and char oxidation,
306 respectively – have similarly high apparent activation energies (124.3 to 171.2 and 108.4
307 to 181.3, respectively), whereas the second regime, representing volatile oxidation and
308 continuing devolatilization is substantially lower (ranging from 16.5 to 50.8 kJ/mol) for
309 all samples. It is not clear that the extraction pre-treatment has any impact on the energy
310 required to initiate combustion of OMW. Jauhiainen⁴⁰ report oxidation activation
311 energies of OMW cake of 153.7, 66.4 and 133.3 kJ/mol for each of three mass loss
312 regimes, in excellent agreement with our results.

313 *Porosity Development via Extraction and Pyrolysis of OMW*

314 BET adsorption isotherms showed a high degree of linearity within the 0-0.35 P/P_0 range,
315 and yielded specific surface areas up to $538 \text{ m}^2/\text{g}_{\text{carbon}}$ for the SCO_2+EtOH OMW (Table
316 5). The specific surface area of the SCO_2 OMW is over 10% greater than the OMW, and
317 the SCO_2+EtOH OWM is over 25% greater than the OMW (Table 5). The pyrolyzed
318 OMW samples are highly mesoporous, conforming to typical type IV isotherms.
319 Interestingly, González⁴⁷ find BET surface areas of only $53 \text{ m}^2/\text{g}_{\text{char}}$, for olive stones
320 pyrolyzed under nitrogen at 600°C for 60 min. On a per gram char basis, our surface
321 areas are over an order of magnitude larger; this is likely due to the considerably larger
322 particles (1-2mm) used by González⁴⁷.

323 In Figure 6, presenting SEM images of raw and extracted OMW samples, we see some
324 evidence of structural change within these samples, namely that the raw OMW are more

325 morphologically heterogeneous with larger particle agglomerates than either of the two
326 SCO₂-extracted samples.

327 *Overview of the proposed biorefinery chain*

328 The over-arching theme of the experimental work was to probe a potential biorefinery
329 chain to improve the possibilities of managing the vast quantities of OMW produced
330 globally. The use of SCO₂ coupled with a polar co-solvent (Ethanol) is to be preferred to
331 the sole SCO₂, as the polarity ensures maximized extraction of bio-phenols. UFA-rich
332 extracts of potential interest in nutraceuticals/pharmaceuticals can be obtained, with
333 interesting concentrations of di-hydroxytyrosol, squalene and other high-value
334 compounds. The extraction treatments (especially SCO₂+EtOH) influenced both
335 oxidation and pyrolysis processes: slight decrease in activation energies, consistent
336 increase in specific surface area and evident structural modifications at level of
337 mesopores. Interestingly, the SCO₂+EtOH flux was found to act as physical/chemical
338 carrier for over 85% of the initial moisture content of the raw OMW. This is of
339 fundamental importance for the efficiency of successive pyrolysis/combustion processes.
340 On the other side, as aqueous fraction is transferred to the obtained extract, heat would be
341 required to freeze-dry it and recover ethanol by distillation. Here, this step, as well as an
342 energetic, mass transfer and economic balance of the overall proposed biorefinery chain
343 is left open for future deepening of this study.

344

345 **Experimental**

346 The OMW samples were obtained from an olive oil processing facility in Andria (BA,
347 Italy). Extraction of polyphenols was carried out using a SCO₂ pilot plant (details
348 follow), granted by Separeco Srl, Italy. Analytical characterizations were carried out at
349 University of Milan. Thermochemical conversion experiments and analysis of chars were
350 carried out at the University of New Hampshire and Boston University.

351 *Supercritical CO₂ Extractions*

352 The polyphenols were extracted from the OMW using a pilot-scale plant (SFE100 Series
353 Plant – Separeco Srl, Italy; Figure S1 in Supplementary Data). The plant contains an
354 extractor of 14 dm³, a gravity separator of 5 dm³, 2 cyclonic separator of 3 dm³, a
355 condenser, a heater and two heat exchangers. The extractions were performed on samples

356 of fresh raw OMW of nearly 7 kgFM, with a density of approximately 0.53 kg dm^{-3} .
357 Extracting conditions were set as follows: pressure 250 bar, temperature $70 \pm 1 \text{ }^\circ\text{C}$, CO_2
358 flow rate 80 kg/h. The extraction was prolonged until no further weight was extracted
359 from the sample. Two types of SCO_2 extractions were tested: one with pure SCO_2 and the
360 other using ethanol as a co-solvent ($\text{SCO}_2 + \text{EtOH}$). Ethanol was added to the biomass in
361 the ratio of 20% w/w, corresponding to a ratio of 0.25% w/w EtOH/CO_2 . Extraction
362 times resulted of 420 and 480 min for SCO_2 and $\text{SCO}_2 + \text{EtOH}$, respectively. After
363 extractions, concentrated extracts were freeze-dried to concentrate fat and phenolic
364 fractions. All extracts and the exhaust OMW obtained were weighed and analyzed to
365 determine their DM and TP contents, to draw a mass balance around the extraction
366 process.

367 *Determination of Phenolic Compounds and Fatty Acids Methyl Esters in OMW and SCO_2* 368 *extracts*

369 The total phenolic compounds (TP) content was determined colorimetrically at 765 nm
370 using Foline-Ciocalteu reagent, according to Singleton⁴⁸, and the results were expressed
371 as gallic acid equivalents (GAE) in $\text{g kg}^{-1}\text{FM}$. The composition of the raw untreated and
372 supercritical fluid extracted olive mill wastes was determined via HPLC on a Finnigan
373 Thermo Surveyor instrument, constituted by a LC Pump Plus, an Autosampler Plus and a
374 PDA Plus diode array detector settled on 280 nm fixed wavelength and in scan mode. A
375 Nova-Pak C18 column (300mm x 3.9mm, $4 \mu\text{m}$ – Waters) was used at room temperature
376 with a 90 min gradient of water/acetic acid (98/2) (solvent A) and 0.5% of acetic acid in
377 water/acetonitrile (solvent B) at a flow rate of 0.8 ml/min and 10 μl injection volume.

378 The gradient program was operated from 10% to 15% of B from 0-10 min, held for 3 min
379 and increased in a linear gradient to 100% (10-65 min).

380 Fatty acids profiles were determined after esterification of lipids and detection by GC-MS
381 analysis (Agilent 6850 Series, Agilent Technologies). The chloroform phase, obtained as
382 reported for the lipids extraction, was evaporated at 30°C using a rotary evaporator under
383 a nitrogen flux. After that, 4 mL of 6% sodium hydroxide dissolved in methanol: dH_2O
384 (4:1 v/v) was added to the sample which was maintained at 60°C for 3 hours in a
385 thermostatic bath. Fatty acids trans-esterification was achieved by adding to the sample 4
386 mL of a boron trifluoride: methanol solution and by heating the sample for 30 min in a

387 vapor recovery system. Esterified fatty acids were extracted twice with 5 mL of hexane. 1
388 μL of each extract was then injected in the GC-MS apparatus, using a non-polar column
389 HP-5 (30 m, 0.25 i.d., 0.25 μm film thickness). Total analysis time was 96.75 min. and
390 the flow rate was 1.20 mL min^{-1} with helium as the carrier gas. Quantification of fatty
391 acids was determined injecting an external multiple standard GRAIN FAME (Supelco).

392 *Activation Energies of Pyrolysis and Oxidation*

393 The exhaust OMW samples were dried and ground in a ball mill and mechanically sieved
394 to yield particles between 125-300 and 300-500 μm . Elemental analysis of carbon,
395 nitrogen and hydrogen contents of each sample was determined by LECO Corporation
396 and reported in Table 3. The apparent activation energies required to pyrolyze and
397 oxidize the raw and extracted OMW samples were measured using non-isothermal
398 thermo-gravimetric analysis over two different heating rates and two particle sizes using
399 a Mettler Toledo TGA/DSC-1. Between 5 and 15 mg of each sample were loaded into a
400 70 μL alumina crucible to achieve a thin layer on the bottom of the pan to prevent mass
401 transfer limitations. Samples were pyrolyzed (or oxidized) under 50 mL min^{-1} of N_2 to
402 provide an oxygen-free environment (and run in air at the same flow rate for oxidation)
403 with nitrogen as the protective gas at 10 mL min^{-1} . The method started by heating the
404 OMW to 110°C and holding it at 110°C for 20 minutes to drive off water and purge the
405 system. The samples were then cooled to 25°C with continual nitrogen (air) flow. The
406 analytical step was carried out under constant nitrogen (air) flow between 25°C and
407 600°C and held at 600°C for 15 minutes, with heating rates of 10°C min^{-1} and 100°C
408 min^{-1} to query the effect of heating rate on the apparent activation energy for each olive
409 waste material. Each sample was repeated 3 times and a standard deviation of the three
410 trials was calculated. The mass of the sample was logged every second to the 10^{-6} grams,
411 along with time and temperature, accurate to 0.01°C.

412 Thermo-gravimetric analysis, or TGA, is often criticized for a lack of applicability to
413 industry because it is often run at relatively slow heating rates (10-25°C/min). However,
414 slower pyrolysis processes are often used to produce a variety of materials and
415 biosynthetic fuels. As such, we query the effect of heating rate on thermal decomposition
416 up to the experimentally reproducible range of our TGA, 100°C/min. While the oxidation
417 reactivities measured here are at lower temperatures compared to small-particle industrial

418 combustion, the particles will likely be within the Zone II kinetics regime at the initial
419 stage of char combustion, shifting to Zone I near 100% burn-out. As such, low
420 temperature measurements are useful in studying the latter stages of burn out for
421 industrial applications, though they cannot be used to describe thermal annealing
422 behavior of the char particles^{49,50}.

423 Many kinetic studies of biomass thermal decomposition show a reaction order close to
424 one; it is common in the biomass literature to apply this global or apparent reaction order
425 to account for all the reactions occurring simultaneously during pyrolysis^{51,52}. By
426 assuming an apparent reaction order of one, this enables determination of the pre-
427 exponential factor (A) and apparent activation energy (E_a) via the Arrhenius equation of
428 the form:

$$429 \quad k = A * \exp\left(-\frac{E_a}{RT}\right) \quad (1)$$

430 where k is the reaction rate constant, R the universal gas constant and T the absolute
431 temperature. The decomposition rate, assuming the mass loss is a result of one or more
432 first-order reactions, is given by equation 2 as:

$$433 \quad \frac{dX(t)}{dt} = k * [1 - X(t)] \quad (2)$$

434 The temperature increases linearly with a constant heating rate seen in equation 3.

$$435 \quad T = T_o(1 + \alpha t) \quad (3)$$

436 Equation 2 can be rewritten taking the heating rate into account to yield equation 4.

$$437 \quad \frac{dX(t)}{dT} = \frac{k}{\alpha} * [1 - X(t)] \quad (4)$$

438 Where α is the constant heating rate $\frac{dT}{dt}$ (K/s) and $X(t)$, the fractional decomposition, is
439 given by:

$$440 \quad X(t) = \frac{m_o - m_t}{m_o - m_c} \quad (5)$$

441 where m_c is the mass at complete decomposition, m_o the initial mass, and m_t the mass at
442 time t . Given the reliance of $X(t)$ on the terminal mass, it is important to clearly identify
443 the final mass after pyrolysis. To do so, samples were held at 600°C until the mass
444 plateaued. The reaction rate constant, k , is a function of temperature; a plot of the natural
445 log of k versus inverse temperature allows the determination of the apparent activation
446 energy and pre-exponential factor. The slope of this plot is equal to $-E_a/R$, and the

447 intercept is $\ln(A)$. The apparent activation energy and pre-exponential factor are key data
448 used to determine the reaction model for a given material. Information that details the
449 dependency of reaction rates on temperature and ramp rate is crucial to designing
450 efficient thermal processing units. The relative rates of decomposition, cracking, and
451 condensation reactions influence the quantity, quality, and long-term stability of biofuel
452 produced ⁵³.

453 *Physical characterization of the materials*

454 Chars of the 125-300 μm particle size samples were prepared in an inert nitrogen
455 environment (100 mL min^{-1} flow rate) in a 1" tube furnace. The samples were heated
456 under nitrogen to and held at 110°C for 1 hour to remove any moisture. The samples
457 were then heated at a rate of 20°C/min to 600°C. The specific surface areas of raw
458 OMW, SCO_2 , and $\text{SCO}_2 + \text{EtOH}$ and pyrolyzed OMW, at particle size fractions of 125-
459 300 μm , were determined using a Micromeritics ASAP 2020 Sorption Analyzer.

460 Approximately 400mg of sample were degassed at 300°C for 10 hours under high
461 vacuum to remove any gases and vapors on the surfaces of the sample. The sample was
462 then transferred from the degasser to the analyzer to determine the surface area and
463 porosity through nitrogen adsorption at 77.35 K using the BET equation. The specific
464 surface area on a per-gram of carbon basis was determined using the carbon content of
465 the samples determined in the TGA oxidation experiments. Morphological changes
466 occurring because of devolatilization were examined via scanning electron microscopy
467 (SEM).

468 **Conclusions**

469 The proposed biorefinery concept was analyzed in detailed aspects of the extraction and
470 the successive energetic valorization, and useful data were obtained. Future work, to
471 determine mass and energy fluxes and define the integration of the considered processes
472 in the proposed biorefinery concept, will address the following key questions:

- 473 1. how much energy (both electric power and heat) is needed for the $\text{SCO}_2 + \text{EtOH}$
474 extraction process, including CO_2 recompression, extract freeze-drying and EtOH
475 recovery?
- 476 2. how much heat is recovered by oxidation of the treated material?

- 477 3. alternatively, how much and what syngas/bio-oil is obtainable by pyrolysis of the
478 treated material?
- 479 4. is the overall biorefinery energy-efficient? With what configuration?
- 480 5. what are the final production costs of the extracts and of the biofuel (syngas or
481 bio-oil) and are they compensated by their economic value?
- 482 6. what is the overall energy balance and feasibility of the proposed biorefinery?
- 483 7. given an economic overview, what is the feasibility, unit costs of energy/biofuels
484 and products possible for this bio-refinery concept?
- 485

486 Acknowledgements

487 The authors appreciate the funding of Veolia Water Solutions and Technologies and the
488 help of Nathalie Martin-Ionesco in promoting this international collaboration. Partial
489 financial support was also granted by Gruppo Ricicla – DISAA, University of Milan,
490 Italy. The authors thank Melissa Lever of Simmons College for assistance with the SEM
491 images. A portion of this material is based upon work supported by the National Science
492 Foundation under Grant No. NSF CBET-1127774.

493

494 References

- 495 ¹ Faostat, <http://faostat3.fao.org/faostat-gateway/go/to/home/E> (accessed November
496 2014)
- 497 ² A.G. Vlyssides, M. Loizides and P.K. Karlis. *J Clean Prod*, 2004, 12, 603-611.
- 498 ³ L. D. Giovacchino, S. Sestili and D. D. Vincenzo. *Eur J Lipid Sci Tech*, 2002, 587-601
- 499 ⁴ L. Lesage-Meessen, D. Navarro, S. Maunier, J. C. Sigoillot, J. Lorquin, M. Delattre, J.
500 L. Simon, M. Asther and M. Labat. *Food Chem*, 2001, 75, 501-507.
- 501 ⁵ M. Niaounakis and C. P. Halvadakis in *Olive Processing Waste Management*; ed.
502 Elsevier Inc.: San Diego, 2006.
- 503 ⁶ S. Martín-Peláez, M.I. Covas, M. Filtó, A. Kušar and I. Pravst. *Mol Nutr Food Res*,
504 2013, 57, 760-71.
- 505 ⁷ R. Capasso, G. Cristinzio, A. Evidente and F. Scognamiglio. *Phytochem*, 1992, 31,
506 4125–4128
- 507 ⁸ G. Ouzounidou, G. I. Zervakis and F. Gaitis. *Terr Aquatic Environ Toxicol* 2010, 22-34.

- 508 ⁹ E. Aranda, I. Sampedro, J.A. Ocampo and I. García-Romera. *Appl Microbiol*
509 *Biotechnol*, 2004, 64, 132-135.
- 510 ¹⁰ Sigma-aldrich, <https://www.sigmaaldrich.com/sigma-aldrich/home.html>, (accessed
511 December 2014)
- 512 ¹¹ Prohealth, https://www.prohealth.com/shop/product.cfm/product__code/PH398,
513 (accessed December 2014)
- 514 ¹² R.W. Owen, A. Giacosa, W.E. Hull, B. Spiegelhalder and H. Bartsch. *Food Chem*
515 *Toxicol*, 2000, 38, 647–59.
- 516 ¹³ A. Shabtay, Y. Hadar, H. Eitam, A. Brosh, A. Orlov, Y. Tadmor, I. Izhaki and Z.
517 Kerem. *Bioresour Technol*, 2009, 100, 6457–6464
- 518 ¹⁴ T. Coskun, E. Debik and N. M. Demir. *Desalination*, 2010, 259, 65–70
- 519 ¹⁵ R. Japón-Luján, J.M. Luque-Rodríguez and M.D. Luque de Castro. *J Chromatogr A*,
520 2006, 1108, 76-82.
- 521 ¹⁶ H. K. Obied, M. S. Allen, D. R. Bedgood, P. D. Prenzler, K. Robards and R.
522 Stockmann. *J Agric Food Chem.*, 2005, 53, 823-837.
- 523 ¹⁷ R. Japón-Luján and M.D. Luque de Castro. *J Chromatogr A*, 2006, 1136, 185-191.
- 524 ¹⁸ F. Le Floch, M.T. Tena, A. Ríos and M. Valcárcel. *Talanta*, 1998, 46, 1123-1130
- 525 ¹⁹ B. Diaz-Reinoso, A. Moure, H. Domingues and J. C. Parajo. *J Agr Food Chem*, 2006,
526 2441–2469
- 527 ²⁰ A. Perez-Galvez, M. Jaren-Galan and M. I. Minguez-Mosquera. In *Handbook of Fruits*
528 *and Fruit Processing*, Ed. Blackwell Publishing: Ames, Iowa, 2006; pp 565-579.
- 529 ²¹ H. J. Vandenburga, A. A. Clifford, K. D. Bartle, J. Carrol, I. Newton, L. M. Garden, J.
530 R. Dean and C. T. Costley. *The Analyst*, 1997, 122, 101R-115R.
- 531 ²² P. Garcia-Salas, A. Morales-Soto, A. Segura-Carretero and A. Fernández-Gutiérrez.
532 *Molecules*, 2010, 15, 8813-8826.
- 533 ²³ P. S. Rodis, V. T. Karathanos and A. Mantzavinou. *J Agr Food Chem*, 2002, 596-601.
- 534 ²⁴ G. A. Baddi, J. Cegarra, G. Merlina, J. C. Revel and M. Hafidi. *J Hazard Mater*, 2009,
535 1119-1123.
- 536 ²⁵ International Energy Agency. World Energy Outlook, Paris, 2008.
537 <http://www.iea.org/media/weowebiste/2008-1994/WEO2008.pdf> (Accessed 27
538 September 2014)
- 539 ²⁶ K. Celis, I. Van Driessche, R. Mouton, G. Vanhoyland and S. Host. *Measur Sci Rev*,

- 540 2001, 1 (1), 177-180.
- 541 ²⁷ C. Di Blasi. *Prog Energy Combust Sci*, 2008, 34, 47-90.
- 542 ²⁸ A. Saddawi, J. M. Jones, A. Williams and M. A. Wojtowicz. *Energ Fuel*, 2010, 24,
543 1274-1282.
- 544 ²⁹ M. J. J. Antal, G. Varhegyi and E. Jakab. *Ind Eng Chem Res*, 1998, 37, 1267-1275.
- 545 ³⁰ J. Chattopadhyay, C. Kim, R. Kim and D. Pak. *Korean J Chem Eng*, 2008, 25 (5),
546 1047-1053.
- 547 ³¹ H. Demiral, I. Demiral, B. Karabacakoglu and F. Tmsek. *Chem Eng Res Des*, 2010,
548 532, 1-8.
- 549 ³² J. M. Encinar, J. F. Gonzalez, G. Martinez and S. Roman. *J Anal and Appl Pyrol*, 2009,
550 85, 197-203.
- 551 ³³ P. Galiatsatou, M. Metaxas, D. Arapoglou and V. Kasselouri-Rigopoulou. *Waste*
552 *Manage*, 2002, 803-812
- 553 ³⁴ C. E. Gokce, S. Guneysu, S. Aydin and S. Arayici. *Open Environ Pollut Toxicol J*,
554 2009, 43-48.
- 555 ³⁵ B.B, Uzun, A.E. Putun and E. Putun. *Energ Fuel*, 2007, 21, 1768-1776.
- 556 ³⁶ F. Adani, 2013. EU Pat, EP20090709779, University of Milan
- 557 ³⁷ S. Laroussi-Mezghani, P. Vanloot, J. Molinet, N. Dupuy, M. Hammami, N. Grati-
558 Kamoun and J. Artaud. *Food Chem*, 2015, 173, 122–132
- 559 ³⁸ D. Grigoriadou, A. Androulaki, E. Psomiadou and M.Z. Tsimidou. *Food Chem*,
560 2007,105 (2), 675–680.
- 561 ³⁹ M. Van de Velden, J. Baeyens, A. Brems and R. Dewil. *Renew Energ*, 2010, 232-242.
- 562 ⁴⁰ J. Jauhainen, J.A. Conesa, R. Font and I. Martn-Gulln. *J Anal Appl Pyrol*, 2004. 72,
563 9-15.
- 564 ⁴¹ A. Ounas, A. Aboulkas, K. El harfi, A. Bacaoui and A. Yaacoubi. *Bioresour Technol*,
565 2011, 102, 11234-11238.
- 566 ⁴² L. Buessing and J.L. Goldfarb. *J Anal Appl Pyrol*, 2012, 96, 78-85.
- 567 ⁴³ A.M. Celaya, A.T. Lade and J.L. Goldfarb. *Fuel Process Technol*, 2015, 129, 39-51.
- 568 ⁴⁴ G. Taralas and M.G. Kontominas. *J Anal Appl Pyrol*, 2006, 76, 109-116
- 569 ⁴⁵ V.B. Agbor, N. Cicek, R. Sparling, A. Berlin and D.B. Levin. *Biotechnol Adv*, 2011,

- 570 29, 675-685.
- 571 ⁴⁶ Y.Z. Zheng, H.M. Lin and G.T. Tsao. *Biotechnol Lett*, 1995, 17, 845-50.
- 572 ⁴⁷ J.F. González, S. Román, J.M. Encinar and G. Martínez. *J Anal Appl Pyrol*, 2009, 85,
573 134-141.
- 574 ⁴⁸ V.E. Singleton, R. Orthofer and R.M. Lamuela-Ravento's. *Method Enzymol*, 1999,
575 299,152–178
- 576 ⁴⁹ M.L. Chan, J.M. Jones, M. Pourkashanian and A. Williams. *Fuel*, 1999, 78, 1539-
577 1552.
- 578 ⁵⁰ J.M. Jones, T.G. Bridgeman, L.I. Darvell, B. Gudka, A. Saddawi and A. Williams.
579 *Fuel Process Technol*, 2012, 101, 1-9.
- 580 ⁵¹ P. Dhepe and R. Sahu. *Green Chem*, 2010, 12, 2153–2156.
- 581 ⁵² P. Parasuraman, R. Singh, T. Bolton, S. Omori and R. Francis. *Bioresources*, 2007,
582 459-471.
- 583 ⁵³ P. A. Webb and C. Orr, in *Analytical Methods in Fine Particle Technology*.
584 Micromeritics Instrument Corporation, 1997.

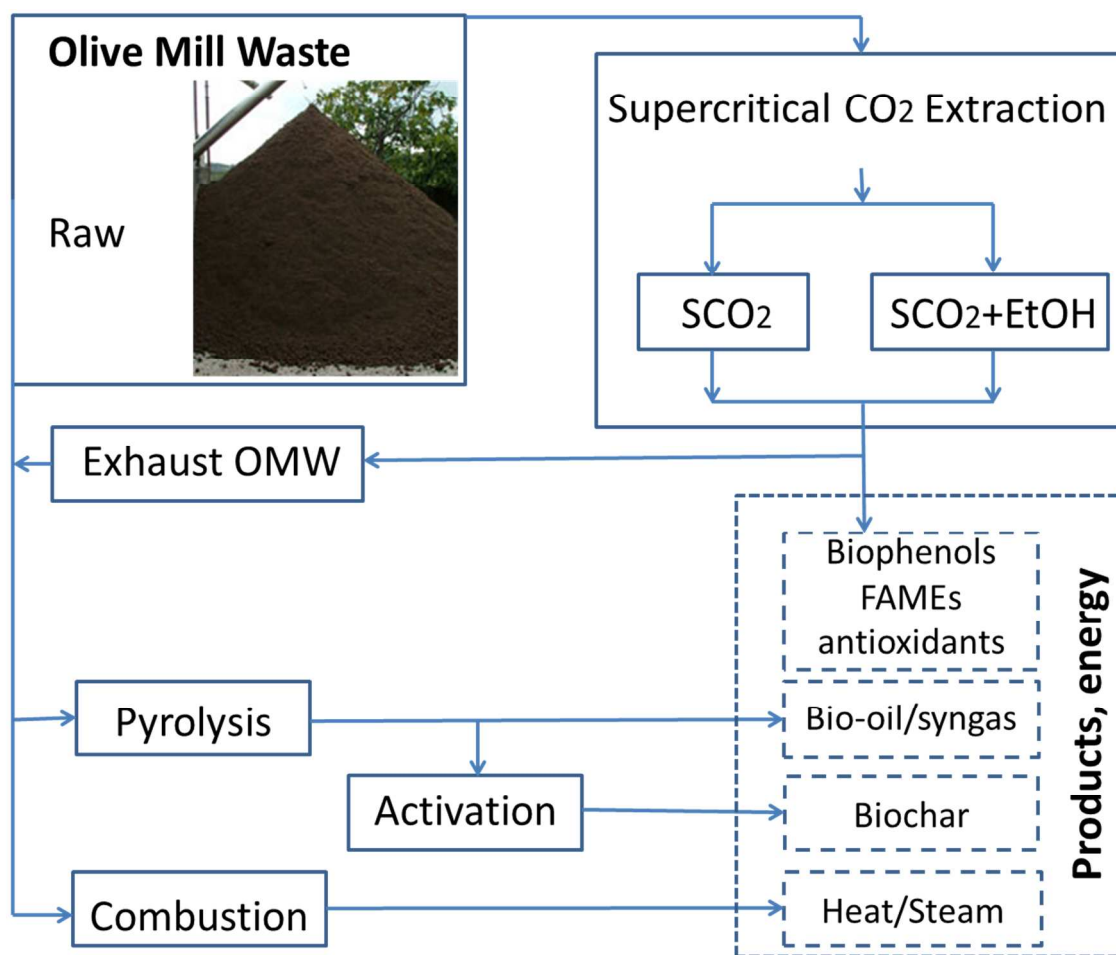
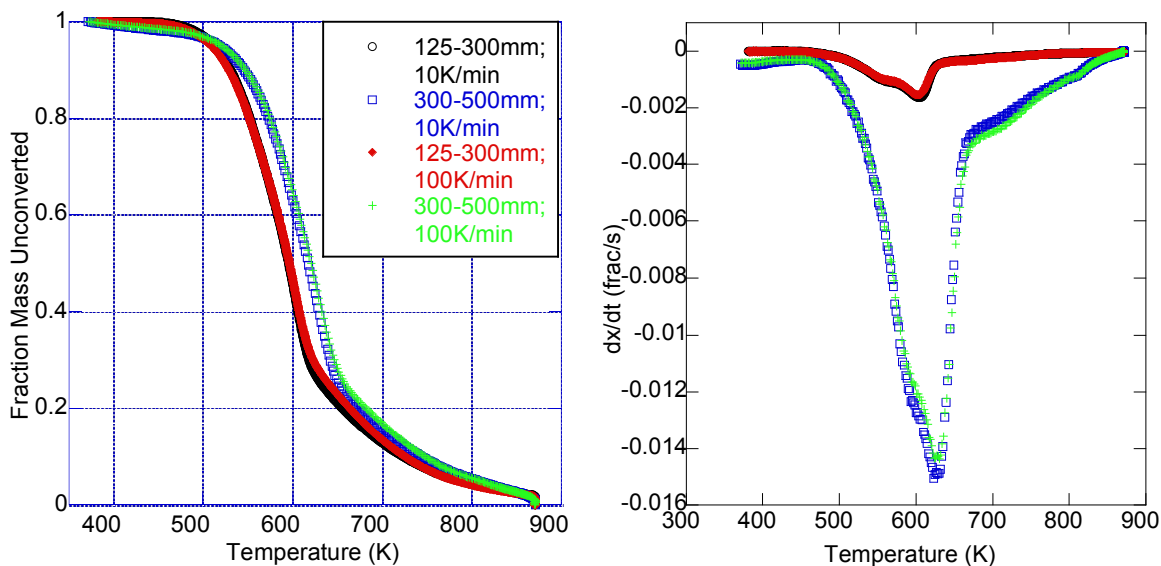


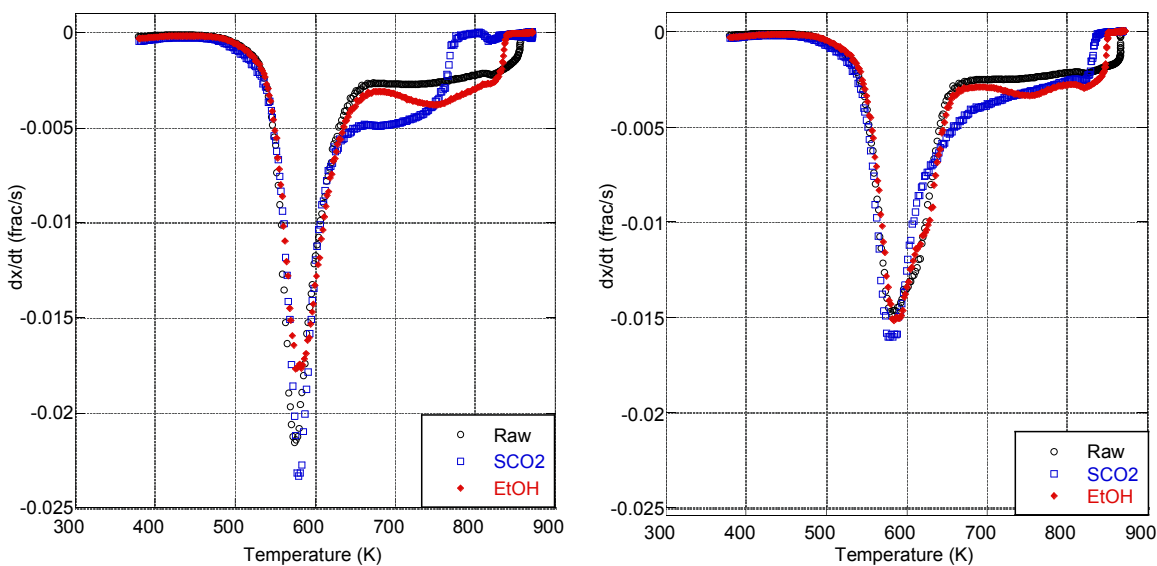
Figure 1. Potential biorefinery pathways for olive mill waste valorization; solid lines indicate OMW treatment paths, dashed lines indicate products recovered from treatment



(a) TG curve (Fraction of mass remaining as a function of temperature)

(b) DTG curve (Rate of fractional mass loss/time as a function of temperature)

Figure 2. Pyrolysis of raw olive mill waste (●) 125-300 μm , 10K/min; (□) 300-500 μm , 10K/min; (♦) 125-300 μm , 100K/min; (+) 300-500 μm , 100 K/min



(a). (●) Raw 125-300 μm , 100K/min; (□) SCO_2 125-300 μm , 100K/min; (♦) $\text{SCO}_2 + \text{EtOH}$ 125-300 μm , 100K/min

(b). (●) Raw 300-500 μm , 100K/min; (□) SCFE 300-500 μm , 100K/min; (♦) EtOH 300-500 μm , 100K/min

Figure 3. DTG curves of oxidation of raw and extracted olive mill waste at 100K/min for (a) 125-300 μm particles and (b) 300-500 μm particles

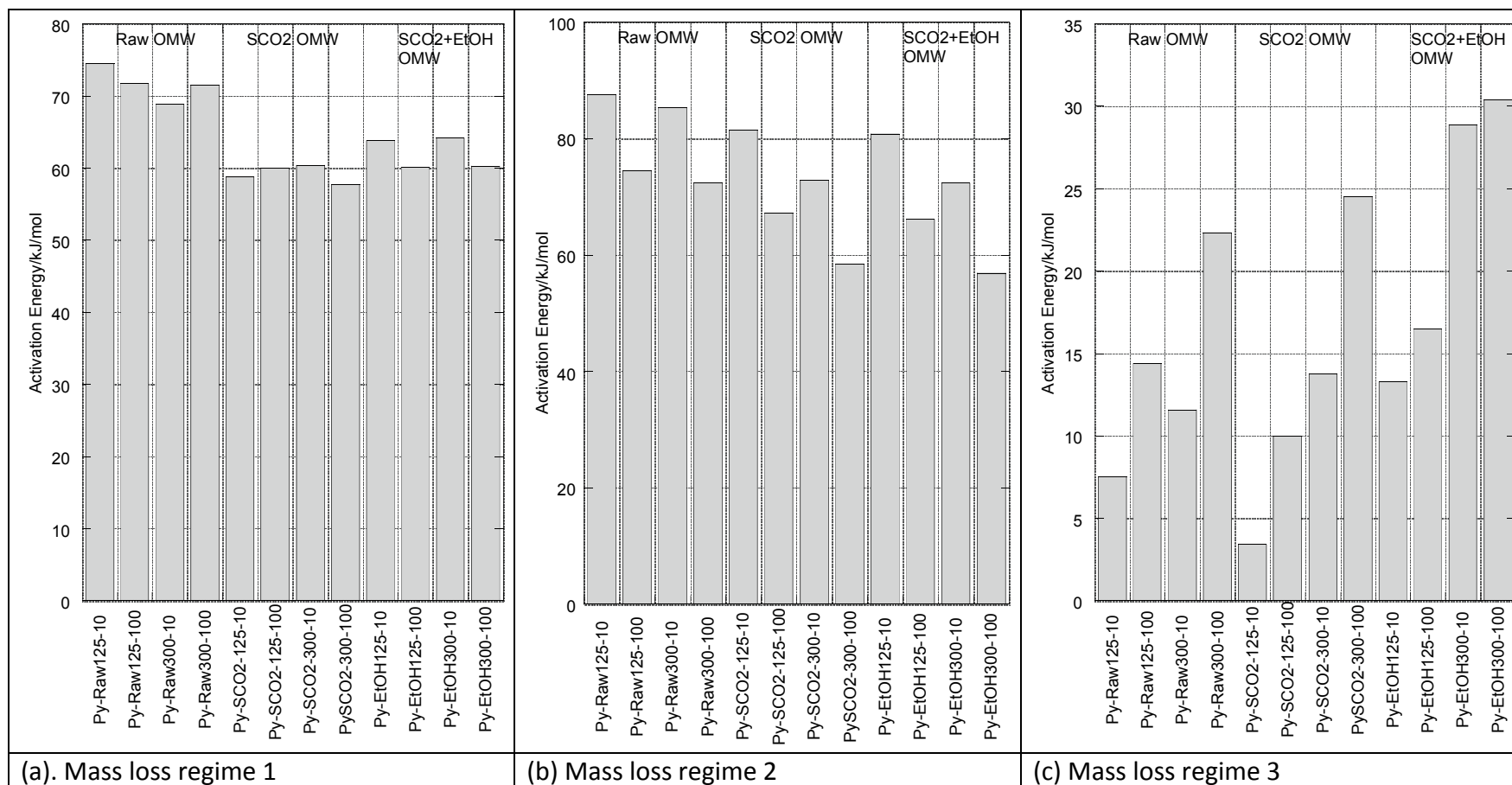


Figure 4. Activation energies of pyrolysis for each mass loss regime [x-axis labels: Treatment (Pyrolysis or Oxidation) – Sample (Raw, SCO₂, SCO₂+EtOH)/Size (125-300 or 300-500 μ m) – Heating rate (10 or 100 K/min)]

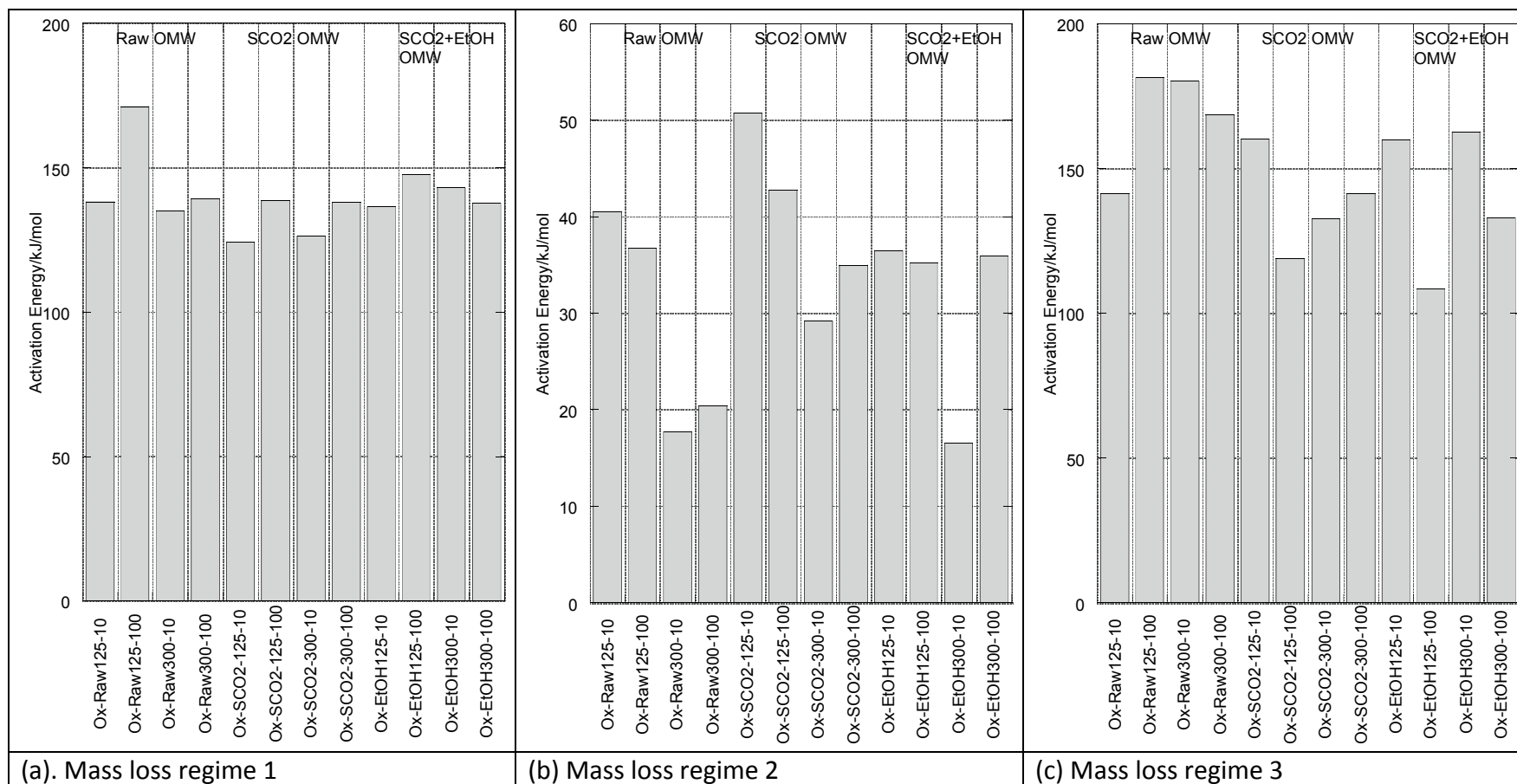


Figure 5. Activation energies of oxidation for each mass loss regime [x-axis labels: Treatment (Pyrolysis or Oxidation) – Sample (Raw, SCO₂, SCO₂+EtOH)/Size (125-300 or 300-500 μm) – Heating rate (10 or 100 K/min)]

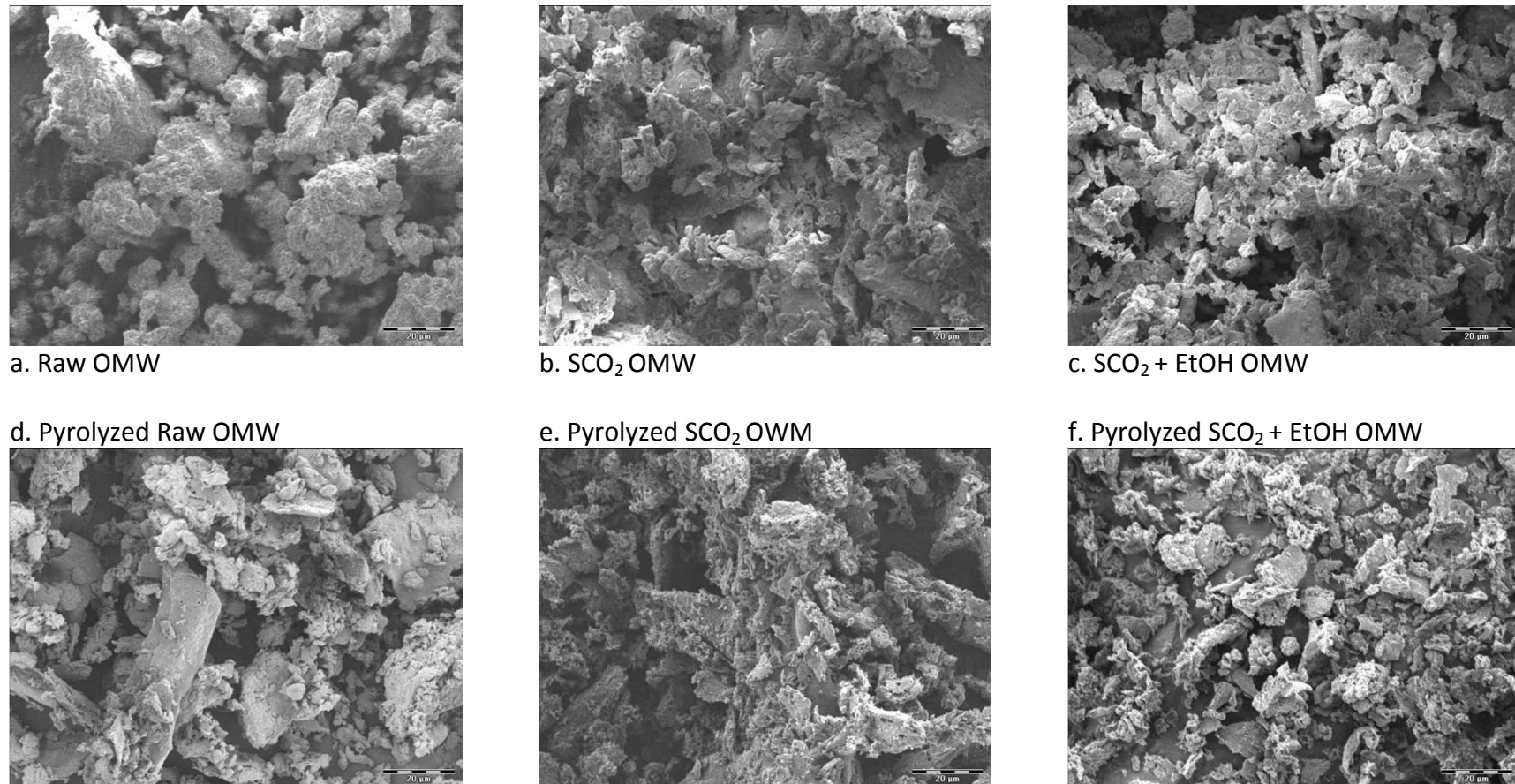


Figure 6. SEM images of raw and extracted olive mill waste biochars (125-300µm) before and after pyrolysis at 600°C

Table 1. Results of SCO₂ and SCO₂+EtOH extractions from raw OMW: concentrations and mass balance of fresh matter (FM), dry matter (DM) and total polyphenols (TP).

	FM balance		DM concentration	DM balance		TP concentration	TP balance			
	kg FM	%	gDM kg ⁻¹ FM	kg DM	%	gGAE kg ⁻¹ FM	g GAE	%		
SCO ₂	Raw Pomace		660	4.818	100	1.809	13.21	100		
	Exhaust Pomace		721	4.405	91.4	2.097	12.81	97.0		
	Extracts	Acqueous extract	1.008	13.8	240	0.242	5.0	0.252	0.25	1.9
		Fat suspension	0.182	2.5	883	0.161	3.3	0.741	0.13	1.0
	Losses		0.016	0.7	-	0.010	0.2	-	0.004	0.03
	Freeze-dried extracts		0.403	5.5	998	0.403	8.4	0.963	0.39	2.9
SCO ₂ +EtOH	Raw Pomace		660	4.792	76	1.809	13.13	100		
	EtOH		1000	1.500	23.8	-	-	-		
	Total		8.760	100	6.292	100				
	Exhaust Pomace		4.390	60.5	947	4.157	66.1	1.611	7.07	53.8
	Extracts	Emulsion (Fat + EtOH + water)	4.230	58.3	487	2.059	32.7	1.420	6.01	45.7
		Losses		0.140	1.9	-	0.075	1.2	-	0.06
	Freeze-dried extracts		0.565	7.7	989	0.559	8.9	10.62	6.01	45.7

Table 2. Phenolic and FAME* contents in dried emulsions extracted (SCO₂ and SCO₂+EtOH) from olive mill waste

Phenolic compounds	SCFE		SCFE+EtOH		FAME*	SCFE		SCFE+EtOH	
	mg kg ⁻¹ DM	% of TP	mg kg ⁻¹ DM	% of TP		g kg ⁻¹ DM	g kg ⁻¹ DM	g kg ⁻¹ DM	g kg ⁻¹ DM
gallic acid	44	4.7	312	3.1	methyl elaidate	451	521		
2,4 dihydroxybenzoic	2	0.3	47	0.5	methyl palmitate	148	210		
4 hydroxybenzoic	10	1.1	117	1.2	cis-Vaccenic acid	69	64		
tyrosol	29	3.1	157	1.6	Methyl 10-ketostearate	59	0		
caffeic acid	5	0.6	85	0.8	methyl stearate	58	51		
chlorogenic acid	78	8.3	759	7.6	Methyl eicosanoate	38	19		
vanillic acid	44	4.7	353	3.5	Methyl palmitoleate	17	17		
syringic acid	34	3.6	246	2.4	Ethyl Oleate	15	0		
di-hydroxytyrosol simil	512	54.1	6046	60.1	methyl linoleate	13	10		
ferulic acid	42	4.4	281	2.8	Methyl behenate	8	7		
trans-p-coumaric acid	8	0.8	104	1.0	Heptadecenoic acid, methyl ester	4	12		
luteolin7p-glucoside	15	1.5	221	2.2	Others	29	16		
Oleuropein-glicone	21	2.2	83	0.8	Total FAME	908	925		
oleuropein	18	1.9	193	1.9	PUFA*	34	20		
cinnammic acid	61	6.4	772	7.7	MUFA*	551	601		
luteolin	22	2.3	274	2.7	SAFA*	315	299		
others	21	2.3	808	8.0	Squalene	21	10		

* FAME = Fatty Acids Methyl Esters; PUFA = Poly-Unsaturated Fatty Acids; MUFA = Mono-Unsaturated Fatty Acids; SAFA = Saturated Fatty Acids

Table 3. Elemental analysis of raw and exhaust OMW samples (with 95% confidence interval, as % w/w on DM)

Sample	%Carbon	%Nitrogen	%Hydrogen
Raw	47.59 ± 0.061	0.14 ± 0.001	6.25 ± 0.042
SCO ₂	47.08 ± 0.061	0.14 ± 0.006	6.35 ± 0.006
SCO ₂ + EtOH	46.82 ± 0.055	0.14 ± 0.006	6.34 ± 0.006

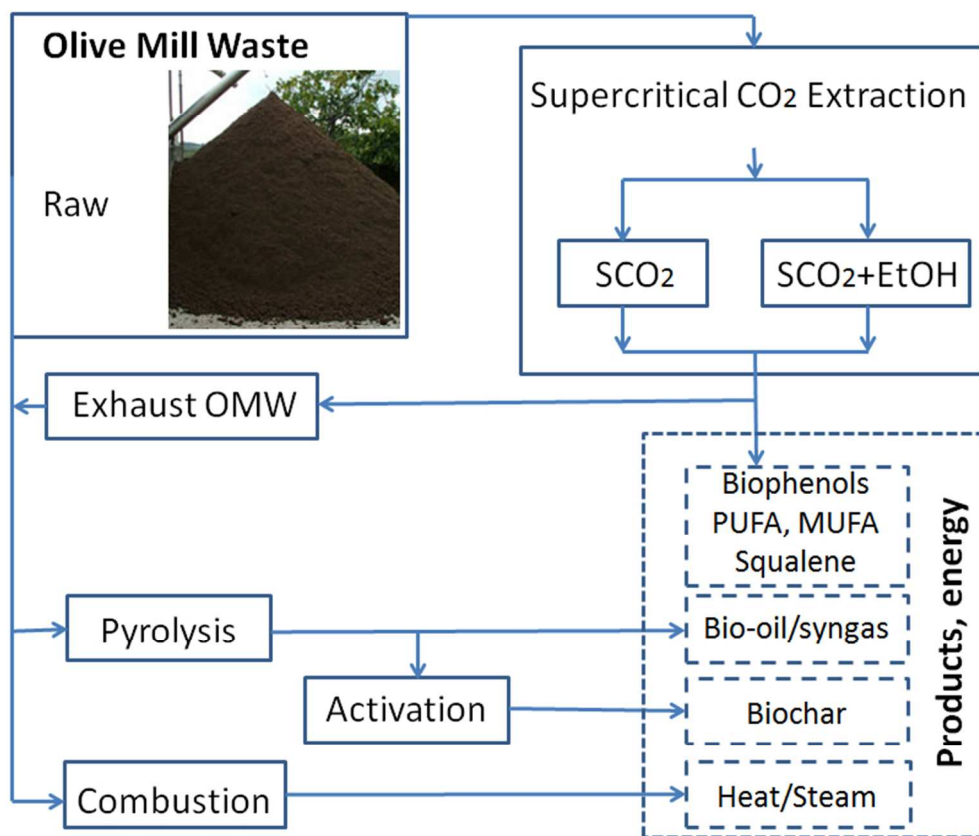
Table 4. Average apparent activation energies of pyrolysis and oxidation over three experimental trials of raw and exhaust OMW (SCO₂ and SCO₂+EtOH) at 10 and 100K/min with associated standard deviations with peak DTG temperature and mass loss rate

Thermal Treatment	Sample	Particle Size Range, mm	Heating Rate, °C/min	Mass Loss Regime 1					Mass Loss Regime 2					Mass Fraction Loss
				Onset Temperature	Endset Temperature	Activation Energy	Pre-exponential Factor	Mass Fraction Loss	Onset Temperature	Endset Temperature	Activation Energy	Pre-exponential Factor	Mass Fraction Loss	
				(K)	(K)	(kJ/mol)	(s ⁻¹)		(K)	(K)	(kJ/mol)	(s ⁻¹)		
Pyrolysis (N ₂)	Raw	125-300	10.0	470.7 ± 0.1	560.1 ± 0.03	74.5 ± 0.7	8.30E+04 ± 1.38E+04	0.30	579.8 ± 0.03	607.8 ± 1.0	87.6 ± 0.2	8.75E+05 ± 3.49E+04	0.38	
			100.0	476.5 ± 0.3	575.8 ± 0.3	71.7 ± 1.1	2.17E+04 ± 5.98E+03	0.27	603.9 ± 0.2	628.3 ± 0.2	74.4 ± 1.6	3.21E+04 ± 9.71E+03	0.38	
		300-500	10.0	470.7 ± 0.05	560.1 ± 0.01	68.9 ± 0.7	2.34E+04 ± 3.64E+03	0.30	579.8 ± 0.03	600.6 ± 2.3	85.3 ± 1.9	5.52E+05 ± 2.17E+05	0.33	
			100.0	476.7 ± 0.1	576.2 ± 0.2	71.5 ± 1.1	2.04E+04 ± 4.63E+03	0.26	609.6 ± 0.3	625.3 ± 0.3	72.4 ± 4.3	2.44E+04 ± 1.70E+04	0.32	
	SCO ₂	125-300	10.0	470.8 ± 0.1	560.1 ± 0.1	58.8 ± 0.6	3.94E+03 ± 2.96E+03	0.30	576.4 ± 0.1	596.9 ± 0.04	81.4 ± 1.0	1.63E+05 ± 1.42E+05	0.33	
			100.0	477.0 ± 0.3	576.2 ± 0.5	60.0 ± 0.3	1.69E+03 ± 9.32E+01	0.27	604.1 ± 0.5	628.4 ± 0.5	67.2 ± 0.9	7.56E+03 ± 1.39E+03	0.37	
		300-500	10.0	470.8 ± 0.05	560.0 ± 0.03	60.4 ± 1.8	3.40E+03 ± 1.27E+03	0.28	576.4 ± 0.03	596.9 ± 0.03	72.8 ± 1.0	3.86E+04 ± 7.07E+03	0.32	
			100.0	487.4 ± 0.5	576.2 ± 0.6	57.7 ± 0.2	9.54E+02 ± 5.11E+01	0.25	604.2 ± 0.6	628.5 ± 0.7	58.4 ± 1.8	1.21E+03 ± 3.83E+02	0.35	
	SCO ₂ +EtOH	125-300	10.0	470.6 ± 0.1	559.9 ± 0.02	63.8 ± 0.9	7.22E+03 ± 1.60E+03	0.28	576.2 ± 0.02	596.7 ± 0.02	80.8 ± 0.4	2.18E+05 ± 1.54E+04	0.33	
			100.0	476.6 ± 0.2	575.6 ± 0.4	60.1 ± 0.3	1.66E+03 ± 1.16E+02	0.26	603.5 ± 0.5	627.7 ± 0.5	66.1 ± 1.6	6.10E+03 ± 1.89E+03	0.37	
		300-500	10.0	470.7 ± 0.03	560.0 ± 0.02	64.2 ± 0.9	7.18E+03 ± 1.35E+03	0.26	576.3 ± 0.02	596.8 ± 0.02	72.3 ± 0.7	3.28E+04 ± 5.34E+03	0.32	
			100.0	477.1 ± 0.4	576.2 ± 0.6	60.3 ± 0.2	1.53E+03 ± 1.04E+02	0.24	604.0 ± 0.6	628.3 ± 0.6	56.9 ± 4.2	1.04E+03 ± 9.38E+02	0.35	
Oxidation (Air)	Raw	125-300	10.0	505.0 ± 0.04	545.0 ± 0.2	138.2 ± 0.9	2.14E+11 ± 5.18E+10	0.27	566.6 ± 0.4	580.7 ± 0.6	40.5 ± 0.3	6.89E+01 ± 2.24E+01	0.33	
			100.0	529.7 ± 0.4	529.7 ± 0.5	171.2 ± 1.0	6.87E+13 ± 1.59E+13	0.39	667.4 ± 0.7	809.1 ± 0.8	36.7 ± 8.5	8.10E+00 ± 1.16E+01	0.50	
		300-500	10.0	504.9 ± 0.04	544.4 ± 0.2	135.1 ± 2.0	1.18E+11 ± 4.94E+10	0.30	565.5 ± 0.3	579.1 ± 0.3	17.7 ± 2.0	7.24E-01 ± 5.04E-01	0.41	
			100.0	529.7 ± 0.5	529.7 ± 0.6	139.2 ± 3.9	5.33E+10 ± 4.59E+10	0.34	666.6 ± 0.2	809.6 ± 0.3	20.4 ± 2.1	1.67E-01 ± 5.84E-02	0.48	
	SCO ₂	125-300	10.0	505.4 ± 0.1	545.2 ± 0.3	124.3 ± 0.8	9.09E+09 ± 1.83E+09	0.26	566.7 ± 0.7	582.3 ± 3.5	50.8 ± 14.0	2.28E+02 ± 3.51E+02	0.35	
			100.0	529.7 ± 0.4	529.7 ± 0.4	138.6 ± 2.1	1.86E+13 ± 3.21E+13	0.39	667.0 ± 1.1	803.5 ± 0.6	42.8 ± 3.4	1.78E+01 ± 5.45E+00	0.56	
		300-500	10.0	505.3 ± 0.1	544.8 ± 0.1	126.3 ± 4.6	1.46E+10 ± 2.26E+10	0.27	565.9 ± 0.2	579.7 ± 0.3	29.2 ± 1.7	7.03E+00 ± 2.58E+00	0.41	
			100.0	529.7 ± 0.1	529.7 ± 0.2	137.9 ± 5.3	4.70E+10 ± 3.59E+10	0.35	666.3 ± 0.5	809.1 ± 0.3	35.0 ± 3.7	4.26E+00 ± 2.70E+00	0.54	
	SCO ₂ +EtOH	125-300	10.0	505.4 ± 0.1	545.6 ± 0.2	136.5 ± 1.8	1.84E+11 ± 8.68E+10	0.32	567.0 ± 0.3	580.9 ± 0.4	36.5 ± 3.4	3.17E+01 ± 3.72E+01	0.34	
			100.0	529.7 ± 0.4	529.7 ± 0.5	147.5 ± 4.6	4.48E+11 ± 4.70E+11	0.36	666.7 ± 0.9	807.6 ± 2.0	35.2 ± 4.1	4.34E+00 ± 2.09E+00	0.58	
		300-500	10.0	505.3 ± 0.04	544.8 ± 0.05	143.1 ± 0.3	7.30E+11 ± 4.20E+10	0.30	565.9 ± 0.1	579.4 ± 0.1	16.5 ± 1.8	5.42E-01 ± 2.02E-01	0.41	
			100.0	529.7 ± 0.2	529.7 ± 0.3	137.6 ± 3.3	2.89E+10 ± 1.73E+10	0.34	665.9 ± 0.3	808.9 ± 0.5	35.9 ± 3.9	3.22E+00 ± 1.73E+00	0.54	

Mass Loss Regime 3						
Onset Temperature	Endset Temperature	Activation Energy	Pre-exponential Factor	Mass Fraction Loss	Peak DTG Temperature	Peak DTG Rate
(K)	(K)	(kJ/mol)	(s ⁻¹)		(K)	(g/s)
639.0 ± 0.03	737.9 ± 0.04	7.5 ± 0.2	3.15E-02 ± 9.46E-03	0.22	605.4	-0.00194
683.1 ± 0.3	731.9 ± 0.3	14.4 ± 1.2	1.13E-01 ± 2.39E-02	0.18	624.4	-0.01513
639.0 ± 0.03	737.8 ± 0.1	11.6 ± 1.9	8.35E-02 ± 2.72E-02	0.27	607.3	-0.00163
683.6 ± 0.4	725.8 ± 0.5	22.3 ± 1.4	4.73E-01 ± 1.22E-01	0.19	630.1	-0.01505
639.0 ± 0.04	737.8 ± 0.02	3.4 ± 0.8	1.81E-02 ± 4.73E-03	0.27	597.8	-0.00171
683.0 ± 0.6	731.8 ± 0.6	10.0 ± 0.6	5.84E-02 ± 5.53E-03	0.19	623.2	-0.01442
639.0 ± 0.03	737.8 ± 0.03	13.8 ± 1.1	1.39E-01 ± 2.68E-02	0.31	601.0	-0.00158
683.2 ± 0.7	732.1 ± 0.7	24.5 ± 1.1	8.23E-01 ± 1.64E-01	0.20	623.2	-0.01302
638.9 ± 0.03	737.8 ± 0.1	13.3 ± 2.6	1.31E-01 ± 6.80E-02	0.29	596.6	-0.00177
682.4 ± 0.7	731.2 ± 0.7	16.5 ± 0.7	1.82E-01 ± 2.01E-02	0.19	625.4	-0.01411
639.0 ± 0.01	738.0 ± 0.02	28.9 ± 3.6	2.42E+00 ± 1.23E+00	0.31	603.2	-0.00165
683.0 ± 0.7	731.9 ± 0.7	30.4 ± 3.6	2.53E+00 ± 1.28E+00	0.23	629.8	-0.01315
641.7 ± 0.3	680.3 ± 0.8	141.2 ± 5.9	3.94E+09 ± 3.57E+09	0.40	553.5	-0.00190
810.7 ± 0.8	847.9 ± 2.8	181.3 ± 9.1	1.52E+10 ± 1.55E+10	0.06	574.1	-0.02193
641.1 ± 0.3	674.8 ± 0.4	180.0 ± 9.0	2.37E+13 ± 3.00E+13	0.30	557.3	-0.00200
811.2 ± 0.3	850.6 ± 0.01	168.4 ± 4.0	7.22E+08 ± 3.72E+08	0.08	582.0	-0.01484
641.1 ± 0.6	676.6 ± 2.6	160.2 ± 8.6	5.19E+11 ± 3.71E+11	0.39	577.3	-0.01020
805.0 ± 0.6	842.1 ± 0.2	118.9 ± 9.4	1.44E+07 ± 1.42E+07	0.01	578.8	-0.02375
641.5 ± 0.2	675.3 ± 0.4	132.6 ± 7.7	2.82E+09 ± 3.53E+09	0.33	559.9	-0.00190
810.7 ± 0.3	830.5 ± 0.8	141.2 ± 17.3	2.49E+07 ± 2.05E+07	0.04	583.6	-0.01637
642.0 ± 0.2	679.3 ± 3.3	160.0 ± 3.9	2.06E+11 ± 2.29E+11	0.34	553.5	-0.00187
809.1 ± 2.1	843.6 ± 1.4	108.4 ± 4.1	8.20E+05 ± 8.30E+05	0.01	580.0	-0.09178
641.4 ± 0.1	674.9 ± 0.2	162.7 ± 8.3	9.63E+11 ± 1.29E+12	0.29	551.6	-0.00211
810.5 ± 0.5	830.9 ± 0.4	133.1 ± 7.6	9.80E+06 ± 9.32E+06	0.04	582.0	-0.01537

Table 5. Surface areas of pyrolyzed chars fabricated from raw and extracted OWM, 125-300 μm , at 10K/min up to 600°C as determined via BET adsorption isotherms

	Carbon Content ($\text{g}_{\text{carbon}}/\text{g}_{\text{sample}}$)	Specific Surface Area per Gram Sample ($\text{m}^2/\text{g}_{\text{char}}$)	Specific Surface Area per Gram Carbon ($\text{m}^2/\text{g}_{\text{carbon}}$)
Raw OMW	0.808	341.5	422.7
SCO ₂ OMW	0.729	344.3	472.3
SCO ₂ + EtOH OMW	0.832	447.9	538.3



High-value extracts for nutraceuticals, biofuels and heat are obtainable from olive mill waste in a new bio-refinery concept that integrates supercritical CO₂ extraction, pyrolysis and oxidation.

216x181mm (96 x 96 DPI)